Chapter 3

PHY Layer Issues — System Imperfections

In this chapter, we investigate signal processing solutions for a few performance-limiting system imperfections in OFDM communications. We first identify a set of key problems whose solutions will enable OFDM radio networks to deliver on its potential; the rest thus balances fundamental investigations with system design and implementation aspects.

To effectively modulate and demodulate OFDM signals, a number of pre- and post-modem tasks must be performed. Signal processing plays an essential role in these tasks. The most important ones among others include

- frequency synchronization
- channel estimation
- phase noise compensation
- peak-to-average power radio (PAPR) reduction
- I/Q imbalance compensation

3.1 Frequency synchronization

The inherent immunity of OFDM to multipath comes at the price of increased sensitivity to inaccurate frequency reference [4] - contrasting to its single-carrier counterparts which are robust to frequency offset but critical to timing inaccuracy. A carrier offset at the OFDM receiver can cause losses in subcarrier orthogonality, and thus introduces interchannel interference (ICI) and severely degrades the system performance [4]. High accuracy carrier offset estimation and compensation is of paramount importance in OFDM communications.

Similar to other communication systems, carrier synchronization in OFDM is usually carried out in two phases, namely, acquisition and tracking. While the acquisition range is the focus during the initial phase, accuracy and stability is the more important design criterion during the tracking stage. In addition, the computational requirements from these two modes are also different. While high cost algorithms are affordable during acquisition, more computationally efficient methods are necessary for the tracking mode.

In many traditional communication systems, a time-domain pilot sequence, $p(1), p(2), \cdots, p(N)$, is inserted periodically and the received signal in the presence of a carrier offset will be

$$p(1)e^{j\phi}, p(2)e^{j\phi+\Delta\omega}, \cdots, p(N)e^{j\phi+\Delta\omega(N-1)} \tag{3.1}$$

The estimation of $\Delta\omega$ is a classic harmonic estimate problem [28] and therefore will not be discussed here. The remainder of this section discusses carrier offset estimation methodologies that exploit the OFDM-specific structural information.

In general, there are two types of OFDM carrier compensation approaches at the baseband, namely, pilot-based and non-pilot based. To ensure an adequate acquisition range, many practical OFDM systems empoly concentrated pilot OFDM symbols (e.g., pilots in IEEE 802.11a and preambles in IEEE 802.16) for initial acquisition. In addition, continuous *pilot subcarriers* are also available for frequency tracking purposes. The obvious advantage of pilot-based approaches is its reliability and accuracy. The non-pilot (or blind) methods estimate the carrier offset by exploiting some known structural information of an OFDM sequence, therefore eliminating the pilot overhead of the systems. Various blind techniques have been proposed to date [7].

In the following we first present the data model of OFDM signals in the presence of carrier offsets. The formulation provides important insight to the impact of imperfect carrier recovery on the demodulation performance. Based on the model established, we present two simple and yet powerful carrier recovery approaches suitable for real world applications.

3.1.1 OFDM carrier offset data model

In the presence of a carrier offset, the time samples of an OFDM signal are modulated by a residual frequency $e^{j\phi n}$. From (2.6), the output vector within the nth demodulation window becomes

$$\mathbf{y}(n) = \mathbf{E}\mathbf{W}_P\mathbf{H}\ \mathbf{s}(n)e^{j\phi(N+L)(n-1)} \tag{3.2}$$

where L is the length of the cyclic prefix and

$$\mathbf{E} = \text{diag}(1,\ e^{j\phi}, \cdots, e^{j(N-1)\phi})$$

In the absence of a carrier offset, applying FFT to the received vector separates signals modulated on different subcarriers as seen in Equation (2.9). On the other hand, since

$$\mathbf{W}_P^H \mathbf{y}(n) = \underbrace{\mathbf{W}_P^H \mathbf{E} \mathbf{W}_P}_{\neq \mathbf{I}} \mathbf{H}\ \mathbf{s}(n) e^{j\phi(N+L)(n-1)}$$

the carrier offset $\mathbf{E}$ matrix destroys the orthogonality among the subchannels. The output on each subcarrier is contaminated by interchannel interference (ICI) from neighboring subcarriers. To recover $\{\mathbf{s}(n)\}$, the carrier offset, ϕ, needs to be estimated and compensated *before* performing the DFT.

3.1.2 Pilot-based estimation

The initial carrier acquisition in OFDM often relies on largely concentrated pilots that are periodically inserted. The simplest scenario involves one or more pilot OFDM symbol(s) with the signal vector $\mathbf{s}$ (modulated on all subcarriers) known to the receiver. In IEEE 802.11a/g and IEEE 802.16d/e for example, dedicated pilots and preambles are available for timing and frequency synchronization.

Assume one pilot OFDM symbol is available. From (3.2), the receiver signal vector is given by

$$\begin{aligned} \mathbf{y} &= \mathbf{E}(\phi)\mathbf{W}_P\mathbf{H}\ \mathbf{s} + \mathbf{n} \\ &= \mathbf{E}(\phi)\mathbf{W}_P\mathbf{S}\mathbf{h} + \mathbf{n} \\ &= \mathbf{U}(\phi)\mathbf{h} + \mathbf{n} \end{aligned}$$

Here we introduce

$$\begin{aligned} \mathbf{S} &= \text{diag}(s_1,\ s_2, \cdots, s_P) \\ \mathbf{U}(\phi) &= \mathbf{E}(\phi)\mathbf{W}_P\mathbf{S} \end{aligned}$$

to facilitate the discussion. $\mathbf{S}$ is known to the receiver whereas $\mathbf{h}$ is the unknown channel vector.

The Maximum Likelihood (ML) estimator for ϕ and $\mathbf{h}$ is

$$(\widehat{\phi}, \widehat{\mathbf{h}}) = \arg_{\phi,\mathbf{h}} \min ||\mathbf{y} - \mathbf{U}(\phi)\mathbf{h}||^2$$

Given that $\mathbf{h}$ is linear with respect to the above minimization, we can express $\mathbf{h} = \mathbf{U}^\dagger(\phi)\mathbf{y}$ and plug it back into the ML estimator as

$$\widehat{\phi} = \arg_{\phi} \min ||\mathbf{y} - \mathbf{U}(\phi)\mathbf{U}^\dagger(\phi)\mathbf{y}||^2$$

The above is a one-dimensional minimization which could be carried out by numerical search.

For tracking purposes, pilots are often only available on a subset of subcarriers locations. In this case, the estimator has to cope with both the unknown channel and the unknown ICI from neighboring subcarriers that carry data information. Joint estimation of all these unknowns is challenging. Fortunately the residual carrier offset during tracking is usually small. Therefore, the ICI can be regarded as additional Gaussian noise.

Under this assumption, (3.2) can be approximated as

$$\mathbf{y}(n) = \mathbf{W}_P \mathbf{H}\, \mathbf{s}(n) e^{j\phi(N+L)(n-1)} + \widetilde{\mathbf{n}}(n)$$

where $\widetilde{\mathbf{n}}(n)$ accounts for both the noise and contributions from the ICI. The first term includes pilot signals that are not affected by the ICI.

Let $\mathcal{P}$ denote the subcarrier indices corresponding to the pilot locations. Clearly, at the location of the pilot subcarriers

$$\mathbf{w}_j^H \mathbf{y}(n) = H(j) s_j(n) e^{j\phi(N+L)(n-1)}, \quad j \in \mathcal{P}.$$

Therefore, one can time differentiate consecutive pilots of the subcarriers in $\mathcal{P}$ to obtain

$$\frac{\mathbf{w}_j^H \mathbf{y}(n)/s_j(n)}{\mathbf{w}_j^H \mathbf{y}(n+1)/s_j(n+1)} = e^{-j\phi(N+L)}, j \in \mathcal{P}; n = 1, ...$$

The residual carrier offset can be readily estimated.

In order to reduce the noise amplification effect due to deep fading channels, the carrier offset estimation must be weighted across all pilot subcarriers based on the channel conditions $H(j), j \in \mathcal{P}$. In addition, smoothing across time n may be unnecessary to avoid instability - see adaptive filtering for more information [11].

3.1.3 Non-pilot based estimation

Non-pilot based approaches can achieve carrier offset estimation without using reference symbols. Instead of using pilot symbols, the frequency offset can also be estimated blindly by exploiting some structural and statistical information of the received signals. For example, Schmidl and Cox proposed a frequency synchronization scheme using OFDM symbols with identical halves [2]. J. van de Beek et al developed an ML estimator by exploiting the redundancy in the cyclic prefix [3].

The technique described here provides a high accuracy carrier estimate by taking advantage of the inherent orthogonality among OFDM subchannels [5].

Indeed, even when the OFDM signal is distorted by an unknown carrier offset, the received signal possesses an algebraic structure which is a direct function of the carrier offset. In particular it is pointed out in Section 2.3 that virtual carriers are often used in OFDM modems to provide guard intervals against neighboring bands. In IEEE 802.11/a/g for example, only 52 out of the 64 subcarriers are used for data modulation. The rest 12 are virtual carriers. In IEEE 802.16e, the number of virtual carriers exceeds 12% of the total number of subcarriers. We show in the following that this property permits the formulation of a cost function which yields a closed-form estimate of the carrier offset.

Recall from (2.9) that $\mathbf{W}_P$ consists of columns of the IDFT matrix corresponding to the used subcarriers. Its orthogonal complement,

$$\mathbf{W}_P{}^{\perp} = [\mathbf{w}_{P+1} \dots \mathbf{w}_N],$$

contains columns of the IDFT matrix corresponding to the virtual carriers. Hence, in the absence of the carrier offset, *i.e.*, $\phi = 0$,

$$\mathbf{w}_{P+i}^H \mathbf{y}(n) = \mathbf{w}_{P+i}^H \mathbf{W}_P \mathbf{H}\, \mathbf{s}(n) = 0, \quad i = 1, \cdots, N-P.$$

Such is not true when $\phi \neq 0$. However, if we let

$$\mathbf{Z} = \begin{bmatrix} 1 & & & 0 \\ & z & & \\ & & \ddots & \\ 0 & & & z^{N-1} \end{bmatrix},$$

it can be easily shown that when $\mathbf{Z} = \mathbf{E}$,

$$\mathbf{w}_{P+i}^H \mathbf{Z}^{-1} \mathbf{y}(n) = \mathbf{w}_{P+i}^H \mathbf{Z}^{-1} \mathbf{E} \mathbf{W}_P \mathbf{H}\, \mathbf{s}(n) = 0 \quad i = 1, \cdots, N-P.$$

This observation suggests that we form a cost function given a finite number of data vectors as follows:

$$P(z) = \sum_{i=1}^{K-P} \sum_{n=1}^{N_p} \left\| \mathbf{w}_{P+i}^H \mathbf{Z}^{-1} \mathbf{y}(n) \right\|^2 \tag{3.3}$$

$$= \sum_{i=1}^{K-P} \sum_{n=1}^{N_p} \mathbf{w}_{P+i}^H \mathbf{Z}^{-1} \mathbf{y}(n) \mathbf{y}^H(n) \mathbf{Z}_{P+i} \tag{3.4}$$

In a system with many virtual carriers, we may choose a portion of the $N-P$ virtual carriers to reduce computational complexity without loss of performance. Clearly, $P(z)$ is zero when $z = e^{j\phi}$. Therefore one can find the carrier offset by evaluating $P(\phi)$ along the unit circle, as in the well-known MUSIC algorithm in array signal processing [6]. On the other hand, it is noted that $P(z)$ forms a polynomial of z with order $2(N-1)$. This allows a closed-form estimate of ϕ through polynomial rooting. In particular, $e^{j\phi}$ can be identified as the root of $P(z)$ on the unit circle.

The algorithm is summarized as follows:

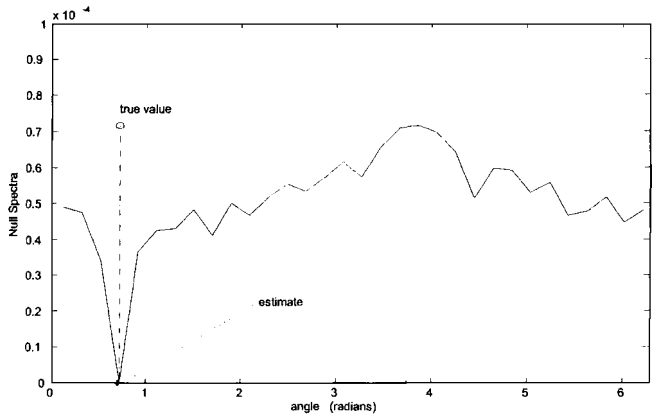

Figure 3.1: The null spectrum of carrier offset estimator

1. Form the polynomial cost function as in (3.3) using the receiver outputs, $\{\mathbf{y}(n)\}$.
2. Estimate the carrier offset as the null of $P(z)$ or the phase of the root of $P(z)$ on the unit circle. In the presence of noise, the carrier offset is estimated as the minima of $P(\phi)$ or the phase of the root of $P(z)$ closest to the unit circle.

The above algorithm takes advantage of the *known* structure of the subspace of OFDM signals and thus offers performance comparable to the subspace-based algorithms with minimum cost. It has been shown that the method is indeed the maximum likelihood (ML) estimate of the carrier frequency offset with a virtual carrier present signal model [8]. More recently, nonlinear least-squares estimators that are robust to correlated noise have been proposed [10].

Example 3 *An example OFDM system with $N = 32$ carriers and $P = 20$ data streams is considered. The carrier offset is estimated using virtual carrier based algorithm described in the previous section. The true frequency offset $\phi = 3.67\Delta\omega$, where $\Delta\omega = \frac{2\pi}{N}$ is the channel spacing. The estimation results using 4 symbol blocks of noise-free data are shown in Fig. 3.1 and Fig. 3.2 In particular Fig. 3.1 shows the null spectrum and Fig. 3.2 displays the root distribution of $P(z)$.*

The minimization of $P(\phi)$ in (3.3) for carrier offset estimation can be implemented adaptively, which readily leads to a carrier tracking algorithm for time-varying environments. Note that no matrix inversion is involved in the cost function, thus excellent transient behaviors of recusive least-squares (RLS) type of adaptive algorithms can be expected with low complexity.

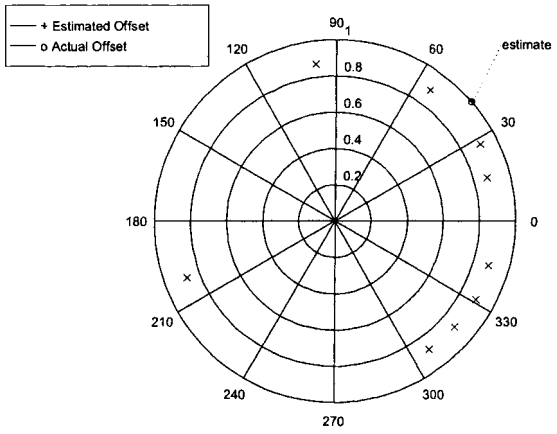

Figure 3.2: The root distribution of polynomial carrier offset estimator

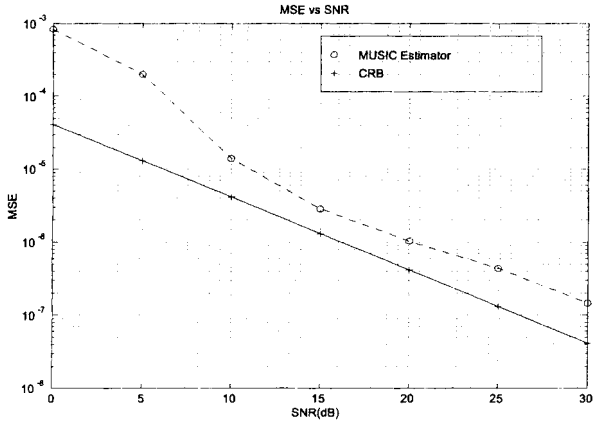

Figure 3.3: Performance of virtual carrier based carrier offset estimator

Example 4 *Figure 3.3 shows the performance of the virtual carrier based frequency estimator. The algorithm uses* 1 *block of data of size* $N = 128$, $P = 68$ *and* $L = 5$. *The true frequency offset* $\phi = \Delta\omega$ *equals the channel spacing. The mean-squared error (MSE) of the carrier offset estimate was obtained by running 200 independent realizations. As seen, the algorithm provides, under reasonable SNR values, very good performance.*

3.2 Channel estimation

To coherently demodulate OFDM signals, channel state information (CSI) must be available at the receiver side. For mobile applications where the radio channel is both time- and frequency-selective (see Section 2.1.4), dynamic channel estimation is necessary. The literature on OFDM channel estimation is abundant, most of which addresses channel estimation based on pilot tones inserted in the OFDM symbol stream. In [12] for example, the optimum pilot tone spacing is investigated assuming a first order Markov channel. Least-squares (LS) or minimum mean-square error (MMSE) based estimators and their low cost implementation are studied in [13],[14],[17]. Space-time channel estimation suitable for space-time fading channels is investigated in [15]. Parametric-based approaches, which further exploit the channel structure information for better estimation performance, can be found in [16] and reference therein.

In this section, we discuss the basics of statistical OFDM channel estimation and its implementation. Starting with the time-varying OFDM channel model, we first establish the minimum set of conditions for scattered pilots with which channel estimation can be performed. The optimum MMSE channel estimation is then described [13][14], followed by reduced complexity channel estimators that are more suitable for practical implementation.

3.2.1 Pilots for 2D OFDM channel estimation

In reference to Figure 2.11, each OFDM symbol has duration

$$T_{symbol} = (N + L)T_s \text{ seconds}$$

and the subcarrier spacing

$$f_{subcarrier} = 1/NT_s \text{ Hertz}$$

To facilitate channel estimation, scattered pilots are inserted in the time-frequency grid at pre-determined intervals. An example pilot pattern is illustrated in Figure 3.4. The time (in terms of OFDM symbols) and frequency (in terms of subcarrier spacing) intervals are largely determined by the characteristics of the channels, and in particular its maximum Doppler frequency and the multipath delay spread.

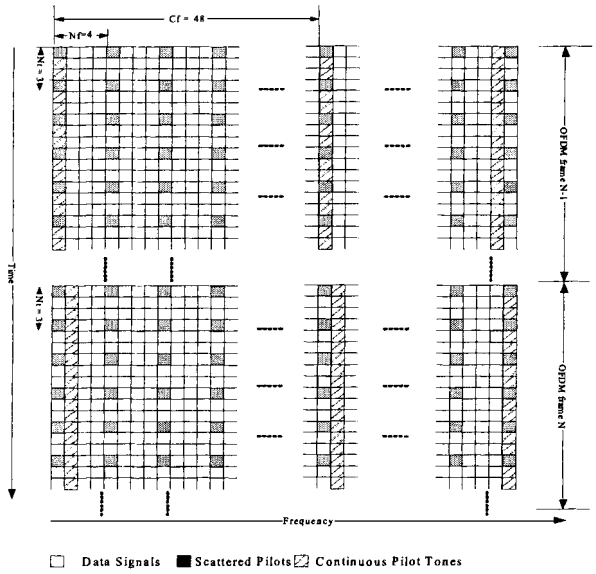

Figure 3.4: An example OFDM pilot structure

Let us assume that

1. The maximum frequency shift is F_D Hz, half of the Doppler bandwidth B_D;
2. The maximum delay spread $\tau_{\max} = LT_s$ seconds;
3. Discrete pilot symbols are placed N_f subcarriers apart in frequency and N_t OFDM symbols apart in time.

To fulfill the sampling theorem in both the time and frequency domains, the pilot spacing (N_f, N_t) must satisfy

$$\text{frequency spacing: } N_f \times f_{subcarrier} < \frac{1}{\tau_{\max}} \Rightarrow N_f < \frac{1}{\tau_{\max} \times f_{subcarrier}} \quad (3.5)$$

$$\text{time spacing: } \frac{1}{N_t T_{symbol}} > 2F_D \Rightarrow N_t < \frac{1}{2T_{symbol} \times F_D} \quad (3.6)$$

Example 5 *The IEEE 802.16e is intended to provide fixed, portable, and mobile broadband wireless services in a wide-area environment with delay spread up*

to $\tau_{\max} = 20\ \mu s$. *The maximum mobility speed anticipated is* $v = 125km/hr$. *In the orthogonal frequency division multiple-access (OFDMA) mode, the subcarrier spacing is designed to be* $f_{subcarrier} = 11.16\ KHz$ *while the OFDM symbol duration is* $100\ \mu s$[7].

- *The maximum frequency domain spacing for the pilots is*

$$N_f < \frac{1}{\tau_{\max} \times f_{subcarrier}} = 5\ \textit{[subcarriers]}$$

- *The Doppler shift at 3.5 GHz carrier frequency is*

$$F_D = \frac{v}{\lambda} = \frac{35m/s}{0.086m} = 408Hz.$$

Therefore, the maximum time domain spacing for the pilots is

$$N_t < \frac{1}{2T_{symbol} \times F_D} = 5\ \textit{[OFDM symbols]}$$

3.2.2 2D MMSE channel estimation

Assuming sufficient pilot symbols are inserted to satisfy the sampling theorem, the next step is to derive a statistical channel estimator for channel responses at all locations. In particular, we are interested in the linear minimum mean-squared error (LMMSE) channel estimator to best fit the channel statistics (known). Recall from (2.2) that the time-frequency channel response of the time-variant channel $h(f,t)$ can be modeled as random processes with covariance matrix:

$$R_h(\Delta f, \Delta t) = E\{h(f;t)h^*(f-\Delta f; t-\Delta t)\} \tag{3.7}$$

The channel statistics can be obtained offline from channel modeling or online from data observations.

In discrete time and frequency, let k and l denote the subcarrier and OFDM symbol indices, respectively. The time-frequency input-output relation in an OFDM system is given by

$$y(k,l) = x(k,l)h(k,l) + n(k,l) \tag{3.8}$$

where $x(k,l), y(k,l)$ and $n(k,l)$ are the transmitted signal, the received signal, and the noise.

Denote the location set of the pilots as $\mathcal{P}$ with corresponding frequency (subcarrier) index m and time (OFDM symbol) index n : $(m,n) \in \mathcal{P}$. In most cases, $\mathcal{P}$ is a small subset of all possible $\{(k,l)\}$. The amount of the pilots presents a tradeoff between channel estimation accuracy and the bandwidth overhead.

Let $r(m,n) = y(m,n)/x(m,n)$ be the normalized received signals at the pilot locations:

$$r(m,n) = h(m,n) + v(m,n); (m,n) \in \mathcal{P} \tag{3.9}$$

The goal of channel estimation is to determine the entire channel response $h(k,l)$ based on a *linear combination* (using 2-D filtering) of the observed pilots:

$$\widehat{h}(k,l) = \sum_{(m,n)\in\mathcal{P}} w(k,l,m,n) r(m,n)$$

Here, $\{w(k,l,m,n)\}$ represent time-frequency variant 2-dimentional filter coefficients. $w(k,l,m,n)$ can be determined using the minimum mean-squared error (Wiener filter) criteria:

$$w(k,l,m,n) = \arg_w \min E\left[|h(k,l) - \widehat{h}(k,l)|^2\right]$$

Theorem 1 *The orthogonality principle: The optimum linear mean-squares estimate $Ax + B$ of random variable y is such that the estimation error $y - (Ax + B)$ is orthogonal to the observation x :*

$$E\{[y - (Ax + B)]x\} = 0.$$

For OFDM channel estimation, the optimal filter coefficients that minimize the MSE are obtained when

$$E\left[(h(k,l) - \widehat{h}(k,l))r^*(m,n)\right] = 0$$

Taking expectations:

$$\underbrace{E[h(k,l)r^*(m,n)]}_{\text{cross}} = \sum_{k',l'\in P} w(k,l,k',l') \underbrace{E[r(k',l')r^*(m,n)]}_{\text{auto}}$$

Both the cross-covariance and the auto-covariance matrices are known *a priori* from Equations (2.2) and (3.9). The coefficients $\{w(k,l,m,n)\}$ can thus be obtained by solving the above linear equation set.

A few observations regarding the 2 dimensional (2D) channel estimator are listed below

- High performance: The above 2D channel estimator is optimum in terms of the MSE given the channel statistics. While further improvements are possible (e.g., parametric based channel estimation where certain channel parameters are assumed to be known [16]), the tradeoff between performance and robustness needs to be carefully evaluated [17].

- High complexity: Note that the computation of the channel response $h(k,l)$ at each location involves 2D filtering of all pilot signals. In addition, the filter coefficients are time- and frequency-dependent as well. Although these coefficients may be calculated offline, the amount of storage and computations required may be prohibitive in practice.

3.2.3 Reduced complexity channel estimation

To alleviate the computational problem, one can either employ a low-rank 2-D estimator or use separable filters that are both 1-dimensional.

The low-rank 2D estimator essentially reduces the 2D filtering to the *vicinity* of the channel response [13]. More specifically,

$$\begin{aligned} \widehat{h}(k,l) &= \sum_{(m,n)\in\mathcal{P}} w(k,l,m,n)r(m,n); \\ w(k,l,m,n) &= 0; \text{ if } |k-m| > \Delta m \text{ or } |l-n| > \Delta n \end{aligned}$$

Δm and Δn are selected based on the channel coherence time and coherence bandwidth, as well as the computation complexity the channel estimator can afford.

Alternatively, the channel estimation complexity can be reduced by partitioning the 2D filtering into separate time-domain filtering and frequency domain filtering. The order with which the two 1-D filtering operations are performed depends on the actual pilot pattern.

Assuming that time-domain filtering is to be carried out first. Dropping the frequency index (k and m) in (3.9) yields

$$r_t(n) = h_t(n) + v_t(n); n \in \mathcal{P}_t \tag{3.10}$$

where $\mathcal{P}_t$ is the time-domain pilot location set. Define

$$\begin{aligned} \mathbf{h}_t &= [\ h(1) \quad h(2) \quad \cdots \quad h(N)\ ]^T \\ \mathbf{r}_{\mathcal{P}_t} &= [\ r(1) \quad r(2) \quad \cdots \quad r(|\mathcal{P}_t|)\ ]^T \\ &= \mathbf{h}_{\mathcal{P}_t} + \mathbf{v}_{\mathcal{P}_t} \end{aligned}$$

as channel responses at all locations and at noisy observations at pilot locations $\mathcal{P}_t$ ($\mathcal{P}_t \ll N$) respectively. The time domain MMSE channel estimation (Wiener filtering) is given by

$$\widehat{\mathbf{h}}_{t,MMSE} = \mathbf{R}_{\mathbf{h}_t\mathbf{h}_{\mathcal{P}_t}} \left(\mathbf{R}_{\mathbf{h}_{\mathcal{P}_t}} + \frac{\mathbf{I}}{SNR} \right)^{-1} \mathbf{r}_{\mathcal{P}_t} = \mathbf{F}_t \mathbf{r}_{\mathcal{P}_t} \tag{3.11}$$

where $\mathbf{R}_{\mathbf{h}_t\mathbf{h}_{\mathcal{P}_t}}$ and $\mathbf{R}_{\mathbf{h}_{\mathcal{P}_t}}$ are the cross and auto channel correlation matrices

$$\begin{aligned}\mathbf{R}_{\mathbf{h}_t\mathbf{h}_{\mathcal{P}_t}} &= E\{\mathbf{h}_t\mathbf{h}_{\mathcal{P}_t}^H\} \\ \mathbf{R}_{\mathbf{h}_{\mathcal{P}_t}} &= E\left\{\mathbf{h}_{\mathcal{P}_t}\mathbf{h}_{\mathcal{P}_t}^H\right\}\end{aligned}$$

$\mathbf{R}_{\mathbf{h}_t\mathbf{h}_{\mathcal{P}_t}}$ and $\mathbf{R}_{\mathbf{h}_{\mathcal{P}_t}}$ are determined by the channel Doppler spectrum and are assumed known to the receiver. Otherwise, the "robust" channel correlation should be used as suggested in [17] if no prior channel knowledge is available).

After time-domain channel estimation, the resulting estimates $\widehat{\mathbf{h}}_{t,MMSE}$ can be used as part of the pilot observations for frequency-domain channel estimation. The effective size of the frequency domain pilot set, $K = |\mathcal{P}_f|$, is therefore increased. In many cases, K is power-of-2 with a comb-type pilot pattern.

Following a similar derivation, we obtain the MMSE estimate of the frequency domain channel response vector as

$$\widehat{\mathbf{h}}_{f,MMSE} = \mathbf{R}_{\mathbf{h}_f\mathbf{h}_{\mathcal{P}_f}}\left(\mathbf{R}_{\mathbf{h}_{\mathcal{P}_f}} + \frac{\mathbf{I}}{SNR}\right)^{-1}\mathbf{r}_{\mathcal{P}_f} = \mathbf{F}_f\mathbf{r}_{\mathcal{P}_f}. \tag{3.12}$$

The computation of the above estimate may be prohibitive in practice if the number of subcarriers, N, is large. To reduce the computations, rearrange the frequency channel response vector into

$$\mathbf{h}_f = \begin{bmatrix} \mathbf{h}_{\overline{\mathcal{P}}_f} \\ \mathbf{h}_{\mathcal{P}_f} \end{bmatrix}$$

where $\mathbf{h}_{\mathcal{P}_f}$ corresponds at the pilot locations and $\mathbf{h}_{\overline{\mathcal{P}}_f}$ is the response vector at other locations. Clearly,

$$\begin{aligned}\widehat{\mathbf{h}}_{\mathcal{P}_f,MMSE} &= \mathbf{R}_{\mathbf{h}_{\mathcal{P}_f}}\left(\mathbf{R}_{\mathbf{h}_{\mathcal{P}_f}} + \frac{\mathbf{I}}{SNR}\right)^{-1}\mathbf{r}_{\mathcal{P}_f} \\ \widehat{\mathbf{h}}_{\overline{\mathcal{P}}_f,MMSE} &= \underbrace{\mathbf{R}_{\mathbf{h}_{\overline{\mathcal{P}}_f}\mathbf{h}_{\mathcal{P}_f}}\mathbf{R}_{\mathbf{h}_{\mathcal{P}_f}}^{-1}}_{\text{interpolation filter}}\widehat{\mathbf{h}}_{\mathcal{P}_f,MMSE}\end{aligned} \tag{3.13}$$

In other words, the frequency channel responses at the pilot locations can be estimated first, whereas the rest can be obtained by interpolation based on these estimates.

Since $\mathbf{h}_{\mathcal{P}_f}$ is the Fourier transform of the finite duration channel impulse response (with most of its energy limited to the maximum delay spread), $\mathbf{R}_{\mathbf{h}_{\mathcal{P}_f}}$ is rank deficient in general. Performing an EVD on $\mathbf{R}_{\mathbf{h}_{\mathcal{P}_f}}$ yields

$$\mathbf{R}_{\mathbf{h}_{\mathcal{P}_f}} = \mathbf{U}\mathbf{\Lambda}\mathbf{U}^H$$

where $\mathbf{U}$ is a unitary matrix and $\mathbf{\Lambda}$ is a diagonal matrix containing $q < K$ non-zero eigen values $\{\lambda_i\}$. If we further assume that all multipath signals are independent, $\mathbf{U}$ reduces to a K-point FFT matrix $\mathbf{W}_K$. As a result,

$$\widehat{\mathbf{h}}_{\mathcal{P}_f,MMSE} = \mathbf{W}_K \begin{bmatrix} \delta_1 & & 0 \\ & \ddots & \\ 0 & & \delta_K \end{bmatrix} \mathbf{W}_K^H \mathbf{r}_{\mathcal{P}_f}$$

$$\delta_i = \begin{cases} \frac{\lambda_i}{\lambda_i + 1/SNR} & i = 1, \cdots, q \\ 0 & i = q+1, \cdots, K \end{cases}$$

Essentially the MMSE estimation is carried out in three steps

1. Step 1: converting the frequency domain observations to the time domain with IFFT: $\mathbf{W}_K^H \mathbf{r}_{\mathcal{P}_f}$;
2. Step 2: weighting and truncating the time-domain channel response based on the multipath delay profile;
3. Step 3: converting the resulting time-domain channel response back to frequency domain with FFT $\mathbf{W}_K$.

Once $\widehat{\mathbf{h}}_{\mathcal{P}_f,MMSE}$ becomes available, several different approaches can be employed to obtain $\widehat{\mathbf{h}}_{\overline{\mathcal{P}}_f}$ through interpolation:

- *MMSE based:* (3.13) provides the MMSE based interpolation that is computationally expensive.
- *FFT based:* The $|\mathcal{P}_f|$-point channel impulse response in Step 2 can be zero-padded into an N-point vector. The upsampled frequency channel response is calculated by applying FFT to the N-point time response vector.
- *Filter based:* linear low-pass interpolation filters can be applied directly to $\widehat{\mathbf{h}}_{\mathcal{P}_f,MMSE}$. Essentially the interpolation is performed by inserting $N-|\mathcal{P}_f|$ zeros into $\widehat{\mathbf{h}}_{\mathcal{P}_f,MMSE}$ and then applying a low pass FIR filter. The bandwidth of the filter should be selected based on the coherent bandwidth of the channel.

Figure 3.5 shows the block diagram.

Example 6 *In this example a wireless channel with Doppler shift $F_D = 200Hz$ (120km/s @ 1.8G) and delay spread $Ts = 73$ us ($F_D * Ts = 0.015$) is considered. An OFDM system with 256 subcarriers is used. The MSE performance of the channel estimation using three different channel estimation schemes is compared in Figure 3.6. As seen, the 2D algorithm utilizing prior knowledge of the channel yields the best performance. Its performance degrades below that of the 1D approach when no knowledge of the channel is available.*

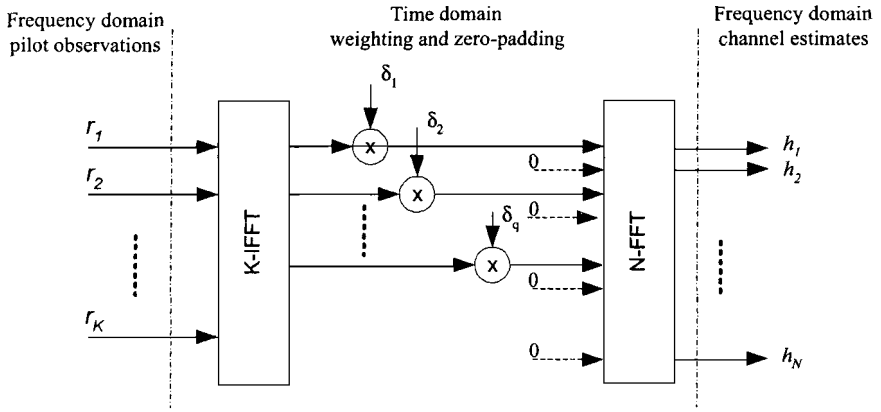

Figure 3.5: A block diagram of FFT-based channel estimation

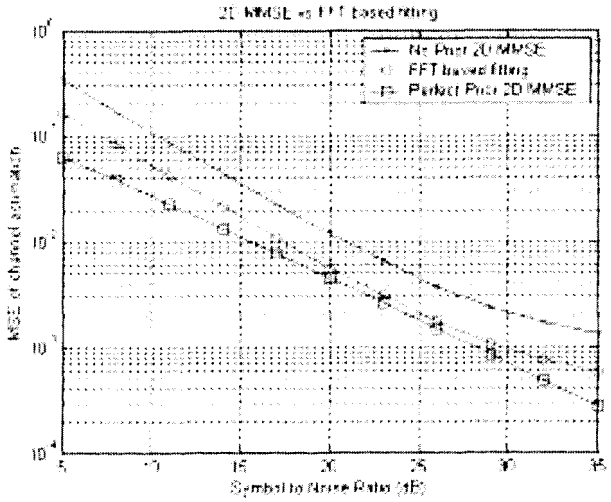

Figure 3.6: Channel estimation performance comparison

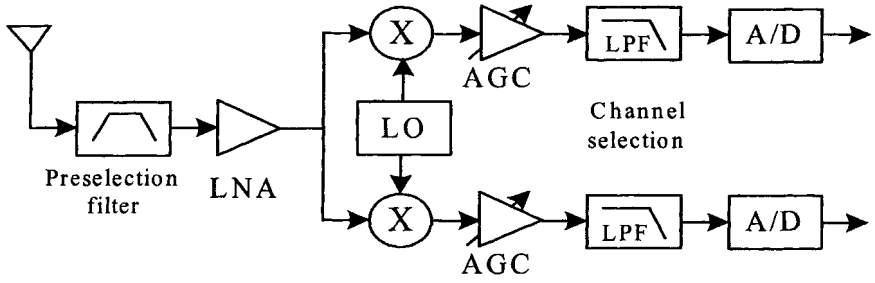

Figure 3.7: A direct-conversion receiver architecture

3.3 I/Q imbalance compensation

To maximize the spectrum efficiency, high-order modulation schemes (e.g., 64-QAM) are used in broadband wireless systems. The combination of OFDM and high order modulation imposes stringent requirements on RF devices [23]. This is particularly true for low-cost direct-conversion RF receivers that suffer from a higher degree of RF imperfections such as the DC-offset and the I/Q imbalance. Sophisticated signal processing algorithms are needed to cope with these RF imperfections in OFDM/high-order QAM.

This section addresses the I/Q imbalance problem in presence of frequency offset. The I/Q imbalance is commonly seen in any RF front-end that exploits analog quadrature down-mixing. This imbalance mainly attributes to the mismatched components in the I and the Q branches. Examples include, but are not limited to, an imperfectly balanced local oscillator (LO) and/or baseband low pass filters (LPF) with mismatched frequency responses. In contrast to an ideal down-converter that performs simple frequency shifting, a down-converter with I/Q imbalance not only down-converts the desired signal, but also introduces its image interference [19][24]. Such image interference, if left uncorrected, presents an error floor which limits the demodulation performance. Moreover, although the I/Q imbalance introduced by the LO may be assumed constant over the signal bandwidth, the mismatches in the subsequent baseband I/Q amplifiers and filters tend to vary with frequencies. Such frequency dependent I/Q imbalance is particularly severe in a wideband direct-conversion receiver and the corresponding estimation and compensation process becomes more challenging [20]. While abundant literature exists on I/Q imbalance compensation (see [19]-[25] and references therein), only a few of them consider the frequency dependent I/Q imbalance [24][20][22][21], let alone the frequency dependent I/Q imbalance in the presence of a frequency carrier offset.

In the following, we first establish a data model for frequency dependent I/Q imbalance and frequency offset. The discussion leads naturally to a receiver

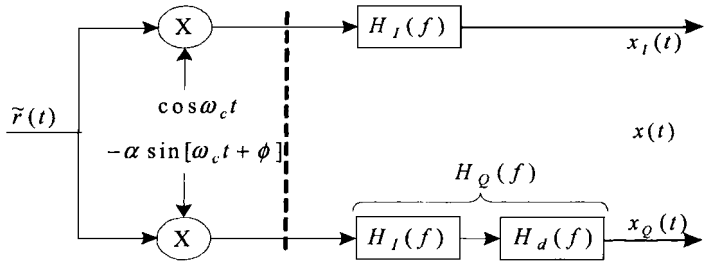

Figure 3.8: An receiver with I/Q imbalance

structure that can compensate both imperfections. To determine the compensation parameters, we introduce a pilot-based scheme for both frequency offset and I/Q imbalance estimation.

3.3.1 I/Q imbalance model

Figure 3.7 shows the general architecture of a direct-conversion receiver. Its mathematical model is given in Figure 3.8. We categorize the I/Q imbalance into a frequency independent part and a frequency dependent part. First, the imbalance caused by the LO can be characterized by an amplitude mismatch α and a phase error ϕ [19]. Since the LO generates a single tone, it is reasonable to model α and ϕ as frequency independent [24][22]. Following the LO are mixers, amplifiers, LPFs and A/D converters, which in general cause the frequency dependent I/Q imbalance. We represent the I/Q baseband signal paths by two mismatched LPFs (with frequency responses of $H_I(f)$ and $H_Q(f)$ respectively) [24]. Using the I channel frequency response as reference, the frequency dependent I/Q imbalance can be modeled by a difference term $H_d(f) = H_Q(f)/H_I(f)$. Since the amplitude mismatch α can be treated as part of the LPF difference $H_d(f)$, we will ignore the effect of α in the ensuing discussion and only consider the frequency independent phase error ϕ and the frequency dependent imbalance $H_d(f)$.

To understand the impact of I/Q imbalance on signal reception, we define the received signal as

$$\tilde{r}(t) = Re\{r(t) \times e^{j(\omega_c+\Delta\omega)t}\} \tag{3.14}$$

$$r(t) = r_I(t) + j \times r_Q(t) = s(t) * c(t) \tag{3.15}$$

where $r(t)$, $s(t)$ and $c(t)$ are the baseband representations of the received signal, the transmitted signal, and the channel response, respectively. $\tilde{r}(t)$ is the received RF signal modulated at center frequency ω_c with a frequency offset $\Delta\omega$.

Following the derivation in [24] and taking into account the initial frequency offset, the down-converted baseband signal $x(t)$ can be represented as

$$\begin{aligned} x(t) &= \mathcal{LPF}\{\tilde{r}(t)e^{-j\omega_c t}\} \quad (3.16) \\ &= r(t)e^{j\Delta\omega t} * h_I(t) \otimes g_+(t) + r^*(t)e^{-j\Delta\omega t} * h_I(t) \otimes g_-(t) \\ &= e^{j\Delta\omega t}s(t) * d(t) + e^{-j\Delta\omega t}s^*(t) * v(t) \quad (3.17) \end{aligned}$$

where

$$\begin{aligned} &g_+(t) = \mathcal{F}^{-1}\{G_+(f)\} = \mathcal{F}^{-1}\{[1 + e^{-j\phi} \cdot H_d(f)]/4\} \\ &g_-(t) = \mathcal{F}^{-1}\{G_-(f)\} = \mathcal{F}^{-1}\{[1 - e^{j\phi} \cdot H_d(f)]/4\} \\ &h_I(t) = \mathcal{F}^{-1}\{H_I(f)\}, \quad h_Q(t) = \mathcal{F}^{-1}\{H_Q(f)\} \\ &d(t) = c(t) * h_I(t) * g_+(t) \\ &v(t) = c^*(t) * h_I(t) * g_-(t). \end{aligned} \quad (3.18)$$

Notice that different from the output of an ideal down-conversion, the desired signal is contaminated by its image interference as seen in Figure 3.9. $d(t)$ is the composite channel for the signal of interest and $v(t)$ quantifies the severity of I/Q imbalance. The signal to image interference ratio is given by

$$SIR = \int_{-\infty}^{+\infty} |d(t)|^2 dt \Big/ \int_{-\infty}^{+\infty} |v(t)|^2 dt \,. \quad (3.19)$$

In practice, the typical image rejection is only around 30dB even with careful design.

After the down-converted signal is digitized at a rate that satisfies the Nyquist sampling theorem, the resulting discrete-time representation of (3.16) is given by

$$x(n) = e^{j\Delta\omega T_s n}s(n) * d(n) + e^{-j\Delta\omega T_s n}s^*(n) * v(n) \quad (3.20)$$

with T_s being the sampling period.

3.3.2 Digital compensation receiver

The above model suggests a compensation receiver depicted in Figure 3.10 where the frequency independent imbalance, the frequency dependent imbalance, and the carrier offset are compensated individually.

Since the frequency dependent imbalance is attributed to the different LPF responses of analog I/Q branches, it can be balanced out with an L-order FIR filter $W(f)$. After the frequency dependent imbalance has been removed, the remaining frequency independent I/Q imbalance and the carrier offset effect can be characterized by a matrix $\mathbf{\Phi}$ as follow:

$$\begin{aligned} \begin{bmatrix} x_I(n) \\ x_Q(n) \end{bmatrix} &= \begin{bmatrix} 1 & 0 \\ -\sin\phi & \cos\phi \end{bmatrix} \begin{bmatrix} \cos\Delta\omega T_s n & \sin\Delta\omega T_s n \\ -\sin\Delta\omega T_s n & \cos\Delta\omega T_s n \end{bmatrix} \begin{bmatrix} r_I(n) \\ r_Q(n) \end{bmatrix} \\ &= \mathbf{\Phi} \begin{bmatrix} r_I(n) \\ r_Q(n) \end{bmatrix} \end{aligned} \quad (3.21)$$

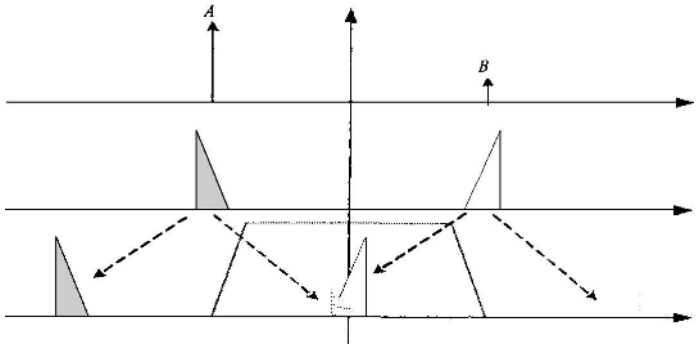

Figure 3.9: Interference caused by I/Q imbalance

where $[r_I(n)\ r_Q(n)]^T$ and $[x_I(n)\ x_Q(n)]^T$ are the baseband representations of the mixer input and output, respectively. The compensation is thus simply left-multiplying the received vector $[x_I(n)\ x_Q(n)]^T$ by $\mathbf{\Phi}^{-1}$, which can be factored into

$$\mathbf{\Phi}^{-1} = \underbrace{\begin{bmatrix} \cos\Delta\omega T_s n & -\sin\Delta\omega T_s n \\ \sin\Delta\omega T_s n & \cos\Delta\omega T_s n \end{bmatrix}}_{frequency\ compensation} \underbrace{\begin{bmatrix} \cos\phi & -\sin\phi \\ \sin\phi & \cos\phi \end{bmatrix}}_{phase\ rotation} \begin{bmatrix} 1/\cos\phi & \tan\phi \\ 0 & 1 \end{bmatrix}. \tag{3.22}$$

Therefore, the $\mathbf{\Phi}^{-1}$ compensation is composed of three terms: the left term corresponds to the frequency offset compensation; the middle term is just a phase rotation and will be absorbed in the channel equalization later on; and the right term suggests a compensation structure that corrects the frequency independent I/Q imbalance with only two multiplication and one addition. We denote this term of the I/Q compensation *asymmetric phase compensator* – similar to the asymmetric form in [25]. It should also be noted that the factorization in (3.22) indicates that the I/Q imbalance be compensated before the frequency offset compensation.

In Figure 3.10, the FIR filter $w(n)$ in the I branch is intended for compensating the frequency dependent imbalance. The $\delta(n - L/2)$ block in the Q branch is simply a delay unit for matching the delay introduced by $w(n)$. Between the dashed lines is the asymmetric phase compensator, where the gain factors a and b correspond to $1/\cos\phi$ and $\tan\phi$ respectively as suggested in (3.22). To further simplify the compensation structure, the gain factor a in the I branch can be merged into $w(n)$ as an additional scaling factor. It is also worth pointing out that without the frequency dependent I/Q imbalance, $w(n)$ reduces to a scalar and the corresponding I/Q compensation structure reduces to the asymmetric compensator as described in [25].

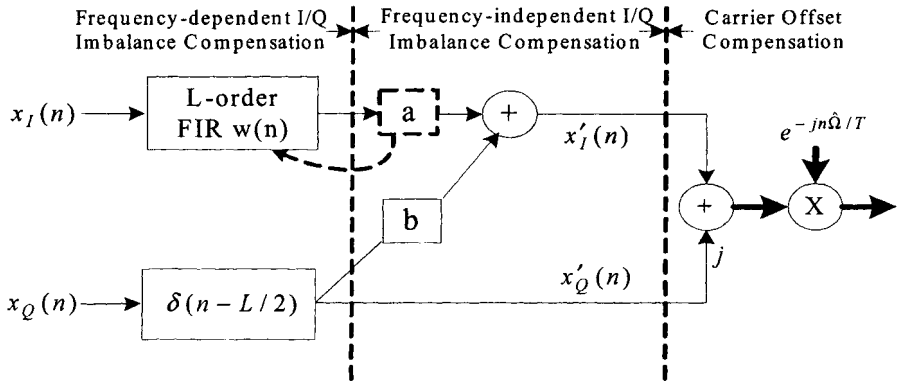

Figure 3.10: Receiver structure for I/Q and carrier offset compensation

3.3.3 Frequency offset estimation with I/Q imbalance

Due to the tangled effect of I/Q imbalance and the frequency offset, determining the parameters for the compensation receiver is nontrivial even with known training symbols. For frequency estimation, the synchronization pilot usually contains several identical symbols. Numerous estimators have been proposed accordingly, e.g., [5] and [26]. Despite their good performance, the accuracy of these estimators degrades in the presence of I/Q imbalance as will be shown later in this section. In the following, we introduce a pilot structure similar to the short SYNCs of IEEE 802.11a and reformulate the problem to take into account the I/Q imbalance. The reformulation leads to a nonlinear least-squares (NLS) based method that can provide accurate estimation even with severe I/Q imbalance.

Figure 3.11 shows the pilot structure for frequency offset and I/Q imbalance compensation. In particular, the pilot contains M identical symbols (each containing N samples, denoted as $p(n)$) with all the even symbols rotated by $\pi/4$. Since the successive pilot symbols are no longer strictly identical (due to the $\pi/4$ rotation), a guard interval (GI) or cyclic prefix (CP) of length P longer than the channel delay spread is introduced to avoid inter-symbol interference (ISI).

To appreciate this pilot pattern, we first examine M identical pilot symbols without the $\pi/4$ phase rotation between pilot symbols. The reason for the additional rotation will become obvious later.

After the GI/CP removal, we stack the received pilot samples in a matrix

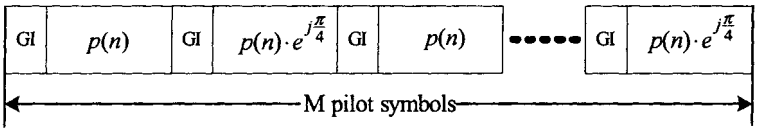

Figure 3.11: Pilot pattern for I/Q imbalance and frequency offset estimation

as follows:

$$\mathbf{X} = \begin{bmatrix} x(1,1) & x(1,2) & \cdots & x(1,N) \\ x(2,1) & x(2,2) & \cdots & x(2,N) \\ \vdots & \vdots & \ddots & \vdots \\ x(M,1) & x(M,2) & \cdots & x(M,N) \end{bmatrix} \tag{3.23}$$

where $x(m,n) = x((m-1)(N+P)+n)$ stands for the nth sample of the mth received pilot symbol. Since the pilot contains M identical symbols, i.e.

$$s(m,n) = p(n), \quad m = 1,2,\cdots,M, \quad n = 1,2,\cdots,N \tag{3.24}$$

where $s(m,n)$ denotes the nth sample of the mth transmitted pilot symbol, (3.20) can be represented as

$$x(m,n) = e^{jm\Omega} \cdot \alpha(n) + e^{-jm\Omega} \cdot \beta(n) \tag{3.25}$$

where

$$\begin{aligned} \alpha(n) &= e^{j\Delta\omega T_s n} p(n) * d(n) \\ \beta(n) &= e^{-j\Delta\omega T_s n} p^*(n) * v(n) \\ \Omega &= \Delta\omega T = \Delta\omega(N+P)T_s \end{aligned} \tag{3.26}$$

and T is the pilot symbol period. Therefore, each column of $\mathbf{X}$ in (3.23), denoted as $\mathbf{x}(n)$, can be expressed as a superposition of two tones as follows:

$$\mathbf{x}(n) = \begin{bmatrix} e^{j\Omega} & e^{-j\Omega} \\ e^{j2\Omega} & e^{-j2\Omega} \\ \vdots & \vdots \\ e^{jM\Omega} & e^{-jM\Omega} \end{bmatrix} \begin{bmatrix} \alpha(n) \\ \\ \beta(n) \end{bmatrix} \stackrel{\text{def}}{=} \mathbf{\Omega} \begin{bmatrix} \alpha(n) \\ \\ \beta(n) \end{bmatrix}. \tag{3.27}$$

The formulation above leads to a classic multi-line spectral estimation problem. Ω is the parameter of interest, while $\alpha(n)$ and $\beta(n)$ are treated as nuisance unknowns. The NLS method described in [28] (maximum likelihood estimator under white Gaussian noise) becomes directly applicable. Particularly in our case, the two frequencies in $\mathbf{x}(n)$ actually contain only one variable with a different sign. As a result, a low cost one-dimension search is sufficient. The frequency estimation can thus be obtained by searching the maxima of the following:

$$\hat{\Omega} = arg \max_{\Omega} \left[tr\{\mathbf{\Omega}(\mathbf{\Omega}^H\mathbf{\Omega})^{-1}\mathbf{\Omega}^H\hat{\mathbf{R}}\} \right] \tag{3.28}$$

where $tr(\cdot)$ denotes the trace of a matrix and $\hat{\mathbf{R}}$ is the sample covariance matrix

$$\hat{\mathbf{R}} = \mathbf{X}\mathbf{X}^H. \tag{3.29}$$

Note that the algorithm proposed in [26] can be considered as a special case of (3.28) in the absence of I/Q imbalance: when $\beta(n) = 0$, (3.28) can be simplified as

$$\hat{\Omega} = arg \max_{\Omega} \left[\mathbf{\Omega}^H \hat{\mathbf{R}} \mathbf{\Omega} \right] \tag{3.30}$$

with $\mathbf{\Omega} \stackrel{\text{def}}{=} \left[e^{j\Omega}\ e^{j2\Omega} \ldots e^{jM\Omega} \right]^T$.

Special attention should be given to $\mathbf{\Omega}$. In our application, $\mathbf{\Omega}$ becomes ill-conditioned when the initial offset is close to zero, which leads to poor estimation accuracy around zero frequency. To maintain a proper condition number regardless of the initial offset, an additional $\pi/4$ rotation can be introduced to all the even pilot symbols. The resulting $\mathbf{\Omega}$ thus becomes always well-conditioned

$$\mathbf{\Omega} = \begin{bmatrix} e^{j\Omega} & e^{-j\Omega} \\ e^{j2\Omega} \cdot e^{j\pi/4} & e^{-j2\Omega} \cdot e^{-j\pi/4} \\ \vdots & \vdots \\ e^{jM\Omega} \cdot e^{j\pi/4} & e^{-jM\Omega} \cdot e^{-j\pi/4} \end{bmatrix}. \tag{3.31}$$

Once the compensation structure is set, the remaining task is to determine the optimum filter coefficients $w(n)$ and the phase compensator b that best remove the I/Q imbalance.

Notice from (3.25) that without I/Q imbalance ($\beta(n) = 0$), the two adjacent received symbols should only differ by a phase rotation, $e^{j\Omega} \cdot e^{\pm\pi/4}$, determined by the carrier offset and the pre-injected rotation. This phase rotation is known to the receiver after the frequency offset has been estimated. However, the presence of I/Q imbalance ($\beta(n) \neq 0$) alters this relationship between the received pilot symbols. This observation suggests a procedure to determine $w(n)$ and b based on such phase rotations. In other words, the optimum $w(n)$ and b can be estimated by minimizing the following:

$$[w(n), b]_{opt} = arg \min_{w(n),b} \left\{ \sum_{m=1}^{M-1} \sum_{n=1}^{N+L-1} \left| x'(m+1, n) - C_m \cdot x'(m, n) \right|^2 \right\} \tag{3.32}$$

where $x'(m,n) = x'_I(m,n) + j \cdot x'_Q(m,n)$ denotes the I/Q compensated signal and C_m represents the phase rotation between adjacent symbols

$$C_m = e^{j\Omega_m} = \begin{cases} e^{j\Omega} \cdot e^{j\pi/4} & : \ m = odd \\ e^{j\Omega} \cdot e^{-j\pi/4} & : \ m = even \end{cases}. \tag{3.33}$$

Note that Ω_m or C_m is considered known by simply substituting Ω with its estimate $\hat{\Omega}$ already obtained in Section 3.3.3.

According to the compensation structure in Figure 3.10, $x'_I(m,n)$ and $x'_Q(m,n)$ are constructed as follows:

$$x'_I(m,n) = x_I(m,n) \otimes w(n) + b \cdot x_Q(m,n) \otimes \delta(n - L/2) \quad (3.34)$$
$$x'_Q(m,n) = x_Q(m,n) \otimes \delta(n - L/2). \quad (3.35)$$

Define the following matrix representations:

$$\mathbf{X}_I(m) = \begin{bmatrix} x_I(m,1) & & & \\ x_I(m,2) & x_I(m,1) & & \\ \vdots & x_I(m,2) & \ddots & \\ x_I(m,N) & \vdots & \ddots & x_I(m,1) \\ & x_I(m,N) & \vdots & x_I(m,2) \\ & & \ddots & \vdots \\ & & & x_I(m,N) \end{bmatrix}_{(N+L-1)\times L}$$
$$\mathbf{x}'_I(m) = [x'_I(m,1)\ x'_I(m,2) \cdots x'_I(m,N+L-1)]^T \quad (3.36)$$

and use similar notations for the Q channel signal (with subscript Q). The I/Q compensation in (3.34) and (3.35) can be rewritten in matrix forms as follows:

$$\mathbf{x}'_I(m) = [\mathbf{X}_I(m) \quad \mathbf{X}_Q(m)\mathbf{1}_L] \begin{bmatrix} \mathbf{w} \\ b \end{bmatrix}$$
$$\mathbf{x}'_Q(m) = \mathbf{X}_Q(m)\mathbf{1}_L \quad (3.37)$$

where

$$\mathbf{w} = [w(1)\ w(2) \cdots\ w(L)]^T$$
$$\mathbf{1}_L = [\underbrace{0 \cdots 0}_{\frac{L-1}{2}}\ 1\ \underbrace{0 \cdots 0}_{\frac{L-1}{2}}]^T. \quad (3.38)$$

Therefore, the two adjacent pilot symbols after compensation are related by

$$\begin{bmatrix} \mathbf{x}'_I(m+1) \\ \mathbf{x}'_Q(m+1) \end{bmatrix} = \begin{bmatrix} \cos\Omega_m & -\sin\Omega_m \\ \sin\Omega_m & \cos\Omega_m \end{bmatrix} \begin{bmatrix} \mathbf{x}'_I(m) \\ \mathbf{x}'_Q(m) \end{bmatrix} + \mathbf{N}(m), \quad (3.39)$$

which can be further expressed as

$$\mathbf{A}(m) \begin{bmatrix} \mathbf{w} \\ b \end{bmatrix} = \mathbf{B}(m) + \mathbf{N}(m) \quad (3.40)$$

where

$$\mathbf{A}(m) = \begin{bmatrix} \mathbf{X}_I(m)\cos\Omega_m - \mathbf{X}_I(m+1) & \mathbf{X}_Q(m)\mathbf{1}_L\cos\Omega_m - \mathbf{X}_Q(m+1)\mathbf{1}_L \\ \mathbf{X}_I(m)\sin\Omega_m & \mathbf{X}_Q(m)\mathbf{1}_L\sin\Omega_m \end{bmatrix}$$
$$\mathbf{B}(m) = \begin{bmatrix} \mathbf{X}_Q(m)\mathbf{1}_L\sin\Omega_m \\ \mathbf{X}_Q(m+1)\mathbf{1}_L - \mathbf{X}_Q(m)\mathbf{1}_L\cos\Omega_m \end{bmatrix} \quad (3.41)$$

and $\mathbf{N}(m)$ stands for the residual error. Stacking $\mathbf{A}(m)$ and $\mathbf{B}(m)$ for all the pilot symbols, the cost function in (3.32) can be minimized by solving the linear least squares equation as follows:

$$\underbrace{\begin{bmatrix} \mathbf{A}(1) \\ \mathbf{A}(2) \\ \vdots \\ \mathbf{A}(M-1) \end{bmatrix}}_{\mathbf{A}} \begin{bmatrix} \mathbf{w} \\ \\ b \end{bmatrix} = \underbrace{\begin{bmatrix} \mathbf{B}(1) \\ \mathbf{B}(2) \\ \vdots \\ \mathbf{B}(M-1) \end{bmatrix}}_{\mathbf{B}} + \begin{bmatrix} \mathbf{N}(1) \\ \mathbf{N}(2) \\ \vdots \\ \mathbf{N}(M-1) \end{bmatrix}$$

The solution of optimum $w(n)$ and b is given by

$$\begin{bmatrix} \mathbf{w} \\ b \end{bmatrix}_{opt} = \mathbf{A}^{\dagger}\mathbf{B} \tag{3.42}$$

where $(\cdot)^{\dagger}$ denotes the matrix pseudo-inverse.

Since the compensation coefficients are determined by restoring the known phase rotation between adjacent pilot symbols, it is also crucial that such rotation structure is robust with respect to the initial frequency offset. This reinforces the necessity of adding a $\pi/4$ rotation to all the even symbols, as mentioned in Section 3.3.3.

It should also be pointed out that for compensating the I/Q imbalance, $w(n)$ can be put in either the I or the Q branch. Similarly, the structure of the asymmetric phase compensator can also be flipped around, i.e., we can instead apply gain a on the Q branch and then a cross path from the I branch to the Q branch with gain b. The purpose of its current arrangement is to avoid the multiplication of $w(n)$ and b. Therefore, the cost function in (3.32) is quadratic, leading to a numerically friendly close-form solution.

Example 7 *In this example, the efficacy of the algorithm is illustrated with hardware test results. The test receiver board consists of all the key components of a direct-conversion receiver as depicted in Figure 3.7. The baseband OFDM waveform is generated by a PC and downloaded to a signal generator with an arbitrary waveform generation function. The signal generator modulates the baseband OFDM waveform to a certain RF frequency and plays it repeatedly with adjustable output power level. The OFDM modulated RF signal is then fed to the test receiver board, where it is down-converted to baseband and digitally sampled. A logic analyzer collects the resulting baseband digital signals and passes them to the PC.*

The OFDM system tested consists of 512 subcarriers with 64QAM coherent demodulation. The frame structure used in the test contains 10 pilot symbols with 16 samples each, followed by the OFDM payload symbols. The signal bandwidth is 4MHz and the RF carrier frequency is set at 1.8GHz in the experiment. Fig. 3.13(a) and Fig. 3.13(b) show the constellation of demodulated signals at

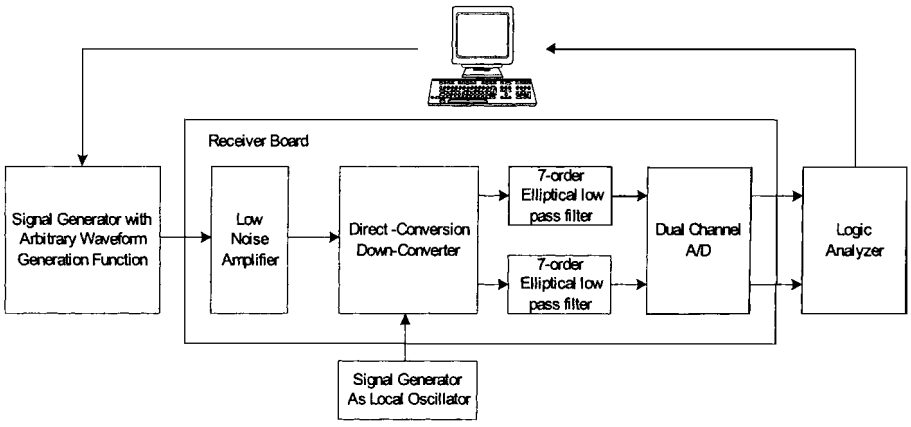

Figure 3.12: Test bench for I/Q imbalance compensation

the input power level of -60dBm. The performance improvement due to the proposed I/Q compensation can be clearly seen, as the original smeared constellation becomes much more distinguishable after the compensation. Fig. 3.14 plots the average SNR of demodulated signals vs. the signal input power. It can be observed that by employing a 5th-order FIR filter, the proposed compensation scheme provides about 4dB SNR improvement at high input signal level. However, if only the frequency independent imbalance is compensated (i.e., reduce the FIR tap to one), the performance gain reduces to 2dB.

3.4 Phase noise compensation

In general, the downconverter induced I/Q imbalance can be calibrated and compensated periodically with large intervals. The phase noise on the other hand, introduces much more rapid distortions to the signals and thus must be coped with in real time.

It is well understood that the phase noise effect on OFDM signal reception consists of two components: an inter-carrier interference (ICI) term that can be modeled as additional Gaussian noise, and a common phase error (CPE) that rotates all the subcarriers equally. While the ICI is difficult to remove due to its noise-like characteristics, the CPE can be easily corrected by estimating such rotation through continuous pilot tones embedded in OFDM symbols [30] [31]. However, existing CPE compensation schemes assume *known channel states* or at least static channels, allowing the CPE to be separated from actual channel

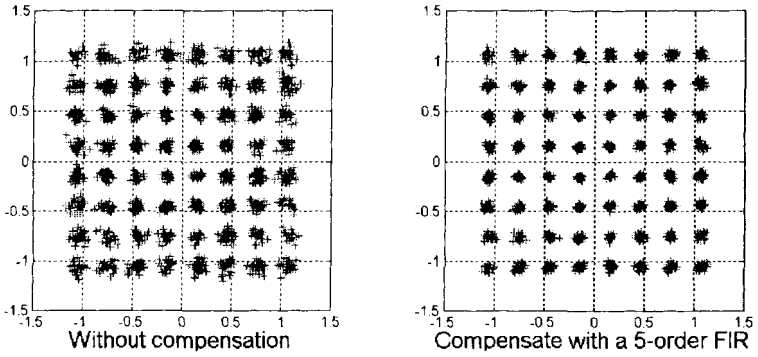

Figure 3.13: OFDM 64-QAM constellation (a) before and (b) after I/Q imbalance compensation

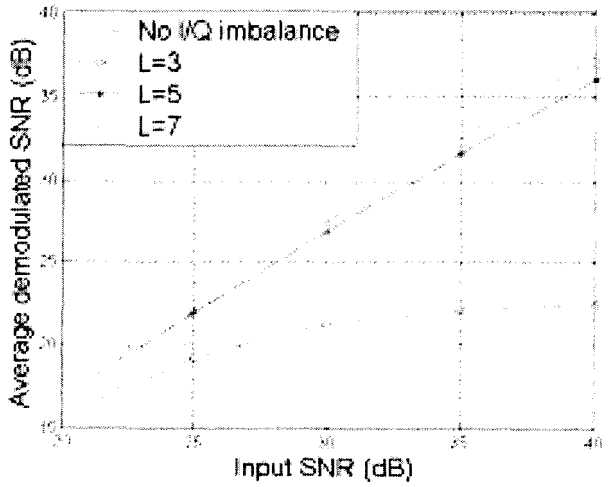

Figure 3.14: Receiver performance with I/Q compensator

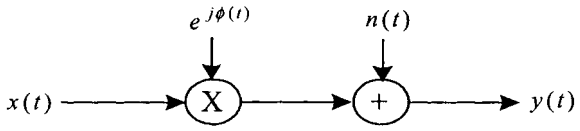

Figure 3.15: Multiplicative phase noise effect

effects. Such an assumption does not hold true for time-varying channels. Reversely, the Wiener filtering channel estimation approaches introduced in Section 3.2 may not be directly applicable in the presence of severe phase noise. Only joint consideration of CPE and channel estimation can address these problems, although in practice the two effects are often dealt with separately.

In this section, the effect of phase noise on channel estimation is first analyzed, based on which the existing time domain MMSE channel estimator is modified to accommodate the CPE. A new CPE estimator suitable for fast fading channels that requires no explicit CSI is then developed based on continuous pilot tones. The estimated CPE, together with the modified MMSE channel estimator, equalizes the composite channel, leading to reception performance close to the CPE-free case.

3.4.1 Mathematical models for phase noise

The phase noise is a multiplicative effect due to the phase variation of the oscillator. To focus on the phase noise only, we assume a simple model in Figure 3.15 where there is no center frequency variation or amplitude fluctuation in the receiver's local oscillator. Therefore, the complex representation of phase noise is given by

$$\eta(t) = e^{j\phi(t)} \simeq 1 + k \cdot \phi(t)$$

The approximation above holds when the phase variation $\phi(t)$ is small, which is the case in most practical applications. $\phi(t)$ is usually modeled as a Gaussian noise with power spectrum density (PSD) $L_\phi(f)$. There are a number of phase noise PSD models in literature [30][33]. Here we choose the one (used in the European dTTb project) that specifies the key parameters of a PLL tracked oscillator [30].

$$L_\phi(f) = 10^{-c} + \begin{cases} 10^{-a} & |f| \le f_1 \\ 10^{-(|f|-f_1)\cdot\frac{b}{f_2-f_1}-a} & |f| \ge f_1 \end{cases}$$

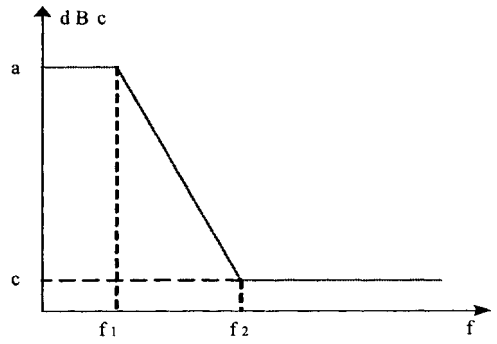

Figure 3.16: Phase noise power spectrum density

As depicted in Figure 3.16, the parameter c determines the PLL noise level, a and f_1 specify the PLL's loop characteristics, while b and f_2 describe how fast the PSD rolls off from the center frequency and where the PSD hits the noise floor, respectively. When an OFDM signal is down-converted by a non-ideal local oscillator with phase noise, the resulting frequency domain signal representation is given by [31]

$$\begin{aligned} y(k,m) &= y(k,m)h(k,m)I_m(0) && (3.43) \\ &\quad + \sum_{l=0;l\neq k}^{N-1} x(l,m)h(l,m)I_{m(l-k)} + v(k,m) && (3.44) \\ &\approx x(k,m)h(k,m)\cdot e^{j\Phi_m} + v_{ICI}(k,m) + v(k,m) \end{aligned}$$

where k and m are the subcarrier index and the symbol index and , respectively. $x(k,m)$, $y(k,m)$ and $h(k,m)$ denote the transmitted signal, the received signal, and the channel response, respectively. $v(k,m)$ is the additive white Gaussian noise. $I_m(l)$ represents the phase noise effect on the OFDM signal reception:

$$I_m(l) = \frac{1}{N}\sum_{l=0}^{N-1} e^{j2\pi nl/N} e^{j\phi_m(n)}$$

As shown in [30][33], the phase noise effect is composed of two parts: (i) a common phase error (CPE) $e^{j\phi_m}$, that rotates all the subcarriers equally (the amplitude variation can be ignored when $e^{j\phi_m}$ is small); and (ii) an inter-carrier interference (ICI) term, v_{ICI}, that is usually modeled as additional Gaussian noise, provided that N is sufficiently large and $x(k,m)$ are mutually independent. Both the CPE and the ICI are shown to be Gaussian variables with variance given as follows [30][33]:

$$\sigma^2_{CPE} = \int_{-B/2}^{B/2} L_\phi(f) \cdot \sin c^2(\pi f T_{symbol}) df$$
$$\sigma^2_{ICI} = \int_{-B/2}^{B/2} L_\phi(f) df - \sigma^2_{CPE}$$

where B is the signal bandwidth and T_{symbol} denotes the OFDM symbol period. Notice from the above expressions that given a certain phase noise spectrum $L_\phi(f)$, there is a trade-off between the CPE and the ICI (by adjusting subcarrier spacing $\frac{1}{T_{symbol}}$). Since the ICI is more difficult to compensate, OFDM system parameters are usually designed in such a way that phase-noise-induced ICI is several dB lower than the operational noise level [29]. For this reason, we will ignore the effect of ICI and only focus on the CPE in the ensuing discussion.

3.4.2 CPE estimation with channel state information

Let us first examine how the phase-noise-induced CPE affects channel estimation in both frequency and time domain filtering.

- In the frequency domain, the CPE adds a phase rotation common to all the subcarriers. Such a rotation presents a constant ambiguity on the actual channel and therefore has no impact on the frequency domain channel estimation/filtering.
- In the time domain, the CPE varies from symbol to symbol with a weak correlation between symbols [30]. As a result, the composite channel $h'(k,m) = h(k,m) \cdot e^{j\Phi_m}$ loses its original low-pass characteristics (determined by the channel Doppler spectrum), which prohibits direct application of the existing time-domain channel estimation/filtering.

As mentioned in earlier sections, pilot OFDM symbols are usually available in practical systems for channel estimation purposes. The samples in the time-frequency grid (various pilot patterns have been considered [34]) allow channel estimation using 2-D or 1+1 D Wiener filtering processes. The same pilots can be utilized for phase noise compensation. In particular, we consider the scenarios with uniformly scattered pilots and continuous pilot tones (over time) exemplified in Figure 3.17. Similar pilot patterns are employed in the DVB-T, IEEE 802.11a/g and IEEE802.16 standards.

After removing the known modulation $x(k,m)$ at pilot locations in (3.43), OFDM channel response in the presence of phase noise can be formulated similar to (3.9) as follows:

$$\begin{aligned} r(k,m) &= h(k,m) \cdot e^{j\Phi_m} + v(k,m) \\ &= h'(k,m) + v(k,m) \end{aligned} \tag{3.45}$$

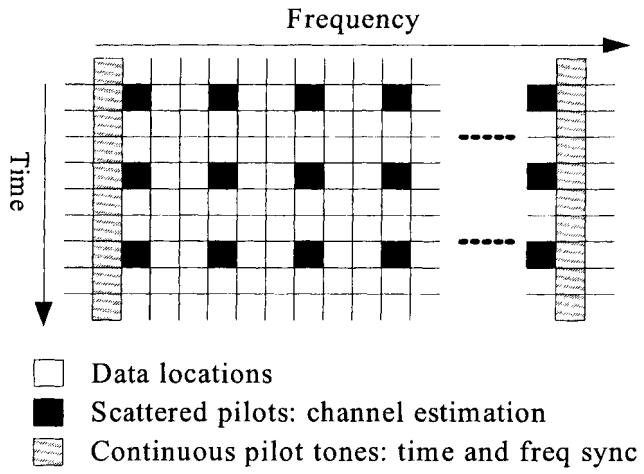

Figure 3.17: Continous and scattered pilots for CPE estimation

where $(k,m) \in \mathcal{P}$ and $\mathcal{P}$ represents the set of pilot locations. $h(k,m), h'(k,m)$ and $r(k,m)$ are the actual channel response, the composite channel response (with CPE), and the channel observation, respectively. $v(k,m)$ now represents white Gaussian noise that incorporates both thermal noise and the phase-noise-induced ICI.

From Section 3.2, channel estimation is essentially an interpolation or filtering of channel responses based on the noisy observations $r(k,m)$ at $(k,m) \in \mathcal{P}$. Unlike the phase-noise free case, we are now dealing with the composite channel $h'(k,m) = h(k,m) \cdot e^{j\Phi_m}$. Therefore, the CPE effect needs to be taken into account for coherent demodulation.

CPE estimation methods based on continuous pilot tones and *known* channel state information have been proposed in [30][31]. In particular, the CPE is estimated as

$$\widehat{\Phi}_m = \angle \left\{ \sum_{k \subset C} r(k,m) h^*(k,m) \right\} \tag{3.46}$$

where C is the set of subcarrier indices of continuous pilot tones. In a time varying channel where the exact channel information is not available, the performance of CPE estimation in (3.46) degrades dramatically. This indicates that for rapid dispersive fading channels the CPE effect and the *time domain* channel response must be estimated jointly.

3.4.3 Time domain channel estimation in the presence of CPE

Since the frequency domain 1-D channel estimation/filtering is not affected by the presence of CPE, one can deal with such tangled effects in two steps. First, we modify the time domain MMSE channel estimator described in Section 3.2.3 to accommodate the CPE effect for composite channel estimation. Then, we develop a CPE estimator that requires no explicit CSI by exploiting continuous pilot tones.

Since CPE only affects time domain filtering, in the ensuing discussion we consider channel estimation at a given subcarrier and drop the frequency index k in (3.45) unless explicitly indicated otherwise.

From Section 3.2.3 on 1-D time domain filtering, we introduce the new channel matrices to take into account the CPE effect as follows,

$$\begin{aligned} \mathbf{h}' &= \mathbf{\Phi}\mathbf{h} \\ \mathbf{h}'_{\mathcal{P}_t} &= \mathbf{\Phi}_{\mathcal{P}_t}\mathbf{h}_{\mathcal{P}_t} \end{aligned}$$

where

$$\begin{aligned} \mathbf{\Phi} &= diag\left\{e^{j\Phi(1)}, e^{j\Phi(2)}, \cdots e^{j\Phi(N)}\right\} \\ \mathbf{\Phi}_{\mathcal{P}_t} &= diag\left\{e^{j\Phi(\mathcal{P}_1)}, e^{j\Phi(\mathcal{P}_2)}, \cdots e^{j\Phi(|\mathcal{P}_t)|}\right\} \end{aligned}$$

Replacing the correlation matrices in (3.11) with the covariance matrices of the composite channel vectors, the MMSE estimate of the composite channel in the presence of CPE needs to be modified to

$$\widehat{\mathbf{h}}_{MMSE} = \mathbf{\Phi}\mathbf{F}_t\mathbf{\Phi}^H_{\mathcal{P}_t}\mathbf{r}_{\mathcal{P}_t} \tag{3.47}$$

where $\mathbf{F}_t$ is defined in (3.11)

The above estimator makes intuitive sense, since it actually suggests that the CPE be first removed from observations at pilot locations before Wiener filtering is applied to smooth out noise. The CPE is then compensated on all the data symbols to obtain the composite channel estimation.

3.4.4 CPE estimation without explicit CSI

Now the problem reduces to determining the CPE without explicit knowledge of the channel information.

Parameters	Specifications
Sampling Frequency (Fs)	4MHz
FFT size	512
Cyclic prefix	64
Scattered pilot spacing (frequency)	3
Scattered pilot spacing (time)	3
# of continuous pilot tones	16
Truncating length of frequency domain MMSE	64
Time domain MMSE block size	20

Table 3.1: OFDM system parameters in joint CPE and channel estimation

Due to its weak time correlation, the CPE must be estimated symbol-by-symbol based on the continuous pilot tones (available in all OFDM symbols). Unlike the approach in (3.46) [30][31], the method described here does not require explicit channel state information. In [35], it is shown that $\mathbf{\Phi}$ can be estimated by minimizing the following:

$$\Phi_0 = \arg\min_{\Phi} E\left\{|\mathbf{\Phi W \Phi}^H \mathbf{R}_{\mathcal{C}} - \mathbf{R}_{\mathcal{C}}|\right\} \tag{3.48}$$

where

$$\mathbf{R}_{\mathcal{C}} = \begin{bmatrix} r(\mathcal{C}_1,1) & r(\mathcal{C}_2,1) & \cdots & r(|\mathcal{C}|,1) \\ r(\mathcal{C}_1,2) & r(\mathcal{C}_2,2) & \cdots & r(|\mathcal{C}|,2) \\ \vdots & \vdots & \ddots & \vdots \\ r(\mathcal{C}_1,N) & r(\mathcal{C}_2,N) & \cdots & r(|\mathcal{C}|,N) \end{bmatrix}$$

contains observations at the continuous pilot location $\mathcal{C}$ over N OFDM symbol periods;

$$\mathbf{W} = \mathbf{R_{hh}}\left(\mathbf{R_{hh}} + \frac{\mathbf{I}}{SNR}\right)^{-1}$$

is a function of the time channel vector covariance matrix $\mathbf{R_{hh}}$.

Example 8 *In this example, the joint CPE and channel estimator is applied to an OFDM system with parameters listed in Table 3.1. The pilot pattern shown in Figure 3.17 is assumed. The UMTS channel (COST207-TU) with different Doppler frequencies is used. The Doppler frequency is fixed at $F_dT_s = 0.05$. We choose the phase noise parameters as suggested in [30] : $a = 6, c = 10.5, f_1 = 1kHz$, and $f_{2=10kHz}$. The MSE of composite channel estimates is used as the performance measure for comparing the following 3 different schemes in rapid dispersive fading channels with phase noise:*

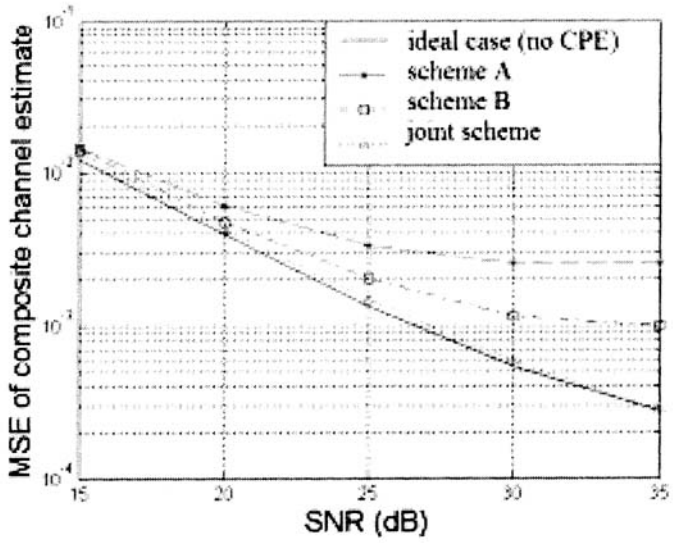

Figure 3.18: Performance of joint phase noise and channel estimation

- *Scheme A: channel estimation with time-domain Wiener filtering as in (3.11) without considering the phase noise effect*
- *Scheme B: channel estimation with time-domain Wiener filtering as in (3.11), followed by the existing CPE estimation as in (3.46)*
- *Joint Scheme: CPE estimation using (3.48), followed by the modified time-domain Wiener filtering as in (3.47)*

From Figure 3.18, it is clear that the presence of CPE causes an irreducible error floor in Schemes A and B. The CPE compensation approach in B does alleviate the CPE effect, however the error floor is only reduced but not eliminated. In contrast, Scheme C with joint CPE and channel estimation performs almost as well as that without CPE.

3.5 Summary

In this chapter, we address OFDM pre- and post- demodulation issues emerging from system imperfections and channel dispersion. Problems related to carrier frequency offset, time- and frequency-selective channels, I/Q imbalance, and phase noise, are formulated. For each problem, we present solutions and algorithms that are practical and efficient. Simulations and application examples are included to show how these techniques can be employed in real OFDM systems.